Nanoscale

Accepted Manuscript

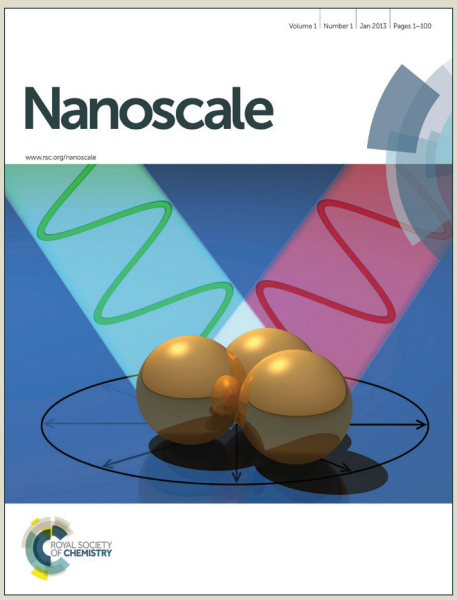

ROYAL SOCIETY OF CHEMISTRY

www.rsc.org/nanoscale

Journal Name

ARTICLE

Ultrathin, Freestanding, Stimuli-Responsive, Porous Membranes from Polymer Hydrogel-Brushes

Received 00th January 20xx,
Accepted 00th January 20xx

DOI: 10.1039/x0xx00000x

www.rsc.org/

Chengjun Kang,[a] Shivaprakash N. Ramakrishna,[a] Adrienne Nelson,[b] Clement V. M. Cremmel,[a] Helena vom Stein,[b] Nicholas D. Spencer,[a] Lucio Isa [b]* and Edmondo M. Benetti [a,c]*

The fabrication of freestanding, sub-100-nm-thick, pH-responsive hydrogel membranes with controlled nano-morphology based on modified poly(hydroxyethyl methacrylate) (PHEMA) is presented. Polymer hydrogel-brush films were first synthesized by surface-initiated atom transfer radical polymerization (SI-ATRP) and subsequently detached from silicon substrates by UV-induced photo-cleavage of a specially designed linker within the initiator groups. The detachment was also assisted by pH-induced osmotic forces generated within the films in the swollen state. The mechanical properties and morphology of the freestanding films were studied by atomic force microscopy (AFM). Inclusion of nanopores of controlled diameter was accomplished by performing SI-ATRP from initiator-coated surfaces that had previously been patterned with polystyrene nanoparticles. Assembly parameters and particle sizes could be varied, in order to fabricate nanoporous hydrogel-brush membranes with tunable pore coverage and characteristics. Additionally, due to the presence of weak polyacid functions within the hydrogel, the membranes exhibited pH-dependent thickness in water and reversible opening/closing of the pores.

Introduction

The fabrication and application of freely suspended polymer films in the sub-100nm thickness range has attracted great theoretical and practical interest over the last decade. Thanks to their high aspect ratios, flexibility, robustness and functional character, these materials have been successfully applied in a variety of technologies, including the development of membranes for molecular-scale separations,[1,2] transducers,[3] actuators[4] and supports for tissue engineering.[5] In several cases, layer-by-layer (LbL) deposition of polymeric components has been exploited to fabricate the films on supporting substrates, from which the "freestanding" membranes could subsequently be released. In LbL formulations the alternated layers are held together by electrostatic, hydrogen bonding, covalent or hydrophobic interactions.[6,7] Despite the versatility of these strategies, they require multiple rinsing steps to ensure structural control over the assembly, whereas LbL films from "weak" interlayer interactions might suffer structural instability and mixing between the components.[6,8] In addition, the thickness of a single component layer is often restricted by a "self-limiting" adsorption process and could not be flexibly tuned, as in the case of polyelectrolytes, where the thickness of a single component layer is typically limited to around 1 nm.[7,8] In an alternative method to fabricate freestanding nano-films, spin coating of polymeric precursor solutions, followed by chemical crosslinking or sol-gel reactions have been employed.[10] In these techniques, polymeric sheets with outstanding mechanical properties could be obtained, where the incorporation of metallic[11] or semiconductor nano- components imparted additional conductive and/or optical properties to the materials.[12]

These limitations have been particularly apparent when the fabrication of ultrathin, freestanding polymeric films with controlled porosities has been attempted. Porous polymeric membranes of sub-100 nm thickness have great potential in membrane technology, for instance in drug delivery or to compartmentalize (bio)chemical reactions.[13] Most of the proposed approaches for fabricating such nano-membranes have suffered from a lack of control over film thickness, especially in the sub-100 nm range and, moreover, the precise tailoring of pore size and density has been challenging. As an example, membranes obtained by phase-inversion of block copolymers have shown very regular porosity on the surface,[14] but the pores became highly tortuous after just a few nanometers. Moreover, even if size and spacing of the pores could be tailored by the block-copolymer architecture, there is limited flexibility to tune one independently of the other.[15,16] These drawbacks can potentially be overcome by applying surface-initiated polymerization (SIP) methods for the synthesis of polymeric films with precisely tunable thickness.[17] In particular, surface-initiated, atom-transfer radical

[a] Laboratory for Surface Science and Technology, Department of Materials, ETH Zurich, Vladimir-Prelog-Weg 5, CH-8093 Zürich, Switzerland.
[b] Laboratory for Interfaces, Soft matter and Assembly, Department of Materials, ETH Zurich, Vladimir-Prelog-Weg 5, CH-8093 Zürich, Switzerland.
[c] Materials Science and Technology of Polymers, MESA+ Institute for Nanotechnology, University of Twente, P.O. Box 217, 7500 AE Enschede, The Netherlands.
E-mail: edmondo.benetti@mat.ethz.ch
† Electronic Supplementary Information (ESI) available See
DOI: 10.1039/x0xx00000x

polymerization (SI-ATRP) has been exploited to graft polymer "brushes" from planar substrates. These can be subsequently detached from the support by a physical or a chemical stimulus.[17] The living character of SI-ATRP ensures a linear growth rate of the grafted brushes and the method is compatible with a large variety of monomers and polymerization media. SI-ATRP-generated polymer brushes with thicknesses ranging from a few tens to several hundreds of nm can be chemically cross-linked, either during the polymerization process itself[18] or by post-modification methods.[19,20] In a similar way, Huck and co-workers synthesized 30-nm-thick, freestanding films of chemically crosslinked poly(glycidyl methacrylate) (PGMA) from initiator-functionalized gold substrates.[19,20] Following an alternative strategy, Jordan et al. fabricated polymer-brush-based "nano carpet" membranes by photochemical crosslinking of self-assembled monolayers of initiators, and subsequent detachment from the substrate.[21]

Although the above-mentioned methods enabled the preparation of brush-based freestanding films with fine control over film thickness, the precise tuning of film morphologies and the introduction of nanopores with controllable diameters and densities have not been accomplished to date. Stimulated by these challenges, we report here a SIP-based fabrication approach to the synthesis of freestanding, nanoporous membranes, featuring full control over all film characteristics, including chemical nature, thickness and porosity. This method couples the "grafting-from" of an in-situ-cross-linked pH-responsive hydrogel-brush[18,22] by SI-ATRP with the self-assembly of particles from liquid interfaces (SALI)[23] as a patterning technique. SI-ATRP was performed from patterned, photo-cleavable, initiator-functionalized surfaces, to produce pH-responsive hydrogel-brushes that could readily be detached from the supporting substrate by a combination of UV-triggered initiator cleavage[24] and osmotic pressure generated within the films in the swollen state.

We have recently introduced photo-cleavable initiator systems, in order to detach polymer brushes from solid substrates and subsequently measure their chain length, polydispersity and grafting density.[24] In the present study, similar assemblies deposited on silicon oxide surfaces have enabled the uniform lift-off of chemically cross-linked brushes. The resulting freestanding hydrogel films could be fabricated in a variety of thicknesses ranging from a few tens to almost 100 nm, with the thickness readily tuned by controlling the SI-ATRP reaction time. Film composition was measured by multiple-transmission-reflection infrared spectroscopy (MTR-IR),[25,26] while morphology and mechanical properties were characterized by atomic force microscopy (AFM). In order to fabricate nanoporous, freestanding hydrogel films, the deposition of the photo-cleavable SI-ATRP initiator was performed on top of previously formed, regular assemblies of polystyrene (PS) nanoparticles (NPs), obtained by the SALI approach. These acted as resist patterns, to selectively inhibit the attachment of initiators on the particle-covered areas. Removal of PS NPs by sonication in toluene produced nanopatterned, initiator-functionalized surfaces, while tuning the particle size and surface coverage enabled the control of diameter and density of the pores in the final membrane. SI-ATRP of hydroxyl ethyl methacrylate (HEMA), in the presence of 5 vol.% of ethyle glycol dimethacrylate (EGDMA), produced cross-linked hydrogel-brush films. The previously masked areas of th substrate led to the creation of nanopores of controlled size and coverage with diameters ranging from 100 to 500 nm throughout the thickness of the film. These films were subsequently functionalized by succinic anhydride (SA), in orde to introduce ionizable carboxylic acid functions. These allowed pH-triggered control of film thickness and reversibl opening/closing of the nanopores within the films. Final lift-off of the surface-grafted hydrogel-brushes was accomplished by a combination of 366 nm UV irradiation to cleave the initiato substrate bond, and basic water treatment, to assist the lift o by osmotic force.

The method reported here allowed the synthesis of ultra-thin freestanding hydrogel membranes with controlled nanoporosities and pH-responsive character. This approach be applied over a large variety of chemistries and enables full control over the films' characteristics. The combination of ATRP and nanoparticle assembly by SALI has thus proved to be a powerful and versatile technique to produce nanopatter freestanding membranes. Such an approach may fin application in the areas of drug delivery and separations technology and the range of porosities can be extended easil to the micron range.

Results and Discussion

Synthesis and Characterization of Freestanding Films

The fabrication of freestanding hydrogel-brush films i illustrated in Fig. 1. In order to graft hydrogel-brushes fron silicon oxide surfaces, the substrates were first coated with (3 aminopropyl) triethoxysilane (APTES)[27] to form a uniform amine-bearing monolayer (see Experimental Section for details). The subsequent reaction with carbonate-activated ((2-bromo-2-methylpropanoyl)oxy) ethyl 4-(4-(1-((((2,5-dioxopyrrolidin-1-yl)oxy) carbonyl)oxy) ethyl)-2-methoxy-5-nitrophenoxy)butanoate (BONMB) allowed the formation o photo-cleavable SI-ATRP initiator layers. BONMB features a bromide-substituted quaternary carbon, which can efficiently act as an ATRP-initiating function, while the dialkoxy nitrobenz group cleaves under 366 nm UV irradiation, generating amine, dioxide and ketone groups.[28] The photo-cleavage reaction o the initiator functions is reported in Fig. 2.

The formation of the APTES and BONMB layers on the silico oxide was monitored by ellipsometry. After APTES deposition, the presence of an organic layer with 0.4 ± 0.1 nm thickness wa recorded. Following the reaction with BONMB, the organic film showed an increase in average thickness, reaching 1.0 ± 0.2 nm. The composition of the BONMB-based initiator monolayer wa further confirmed by MTR-IR spectroscopy.[25,26] As displayed i Fig. 3b, the bands centered at 1665 cm^{-1} and 1741 cm^{-1}, which are characteristic of the formed amide and ester groups BONMB functions, confirmed the successful surfac

immobilization of the photo-cleavable initiator. The main text of the article should appear here with headings as appropriate.

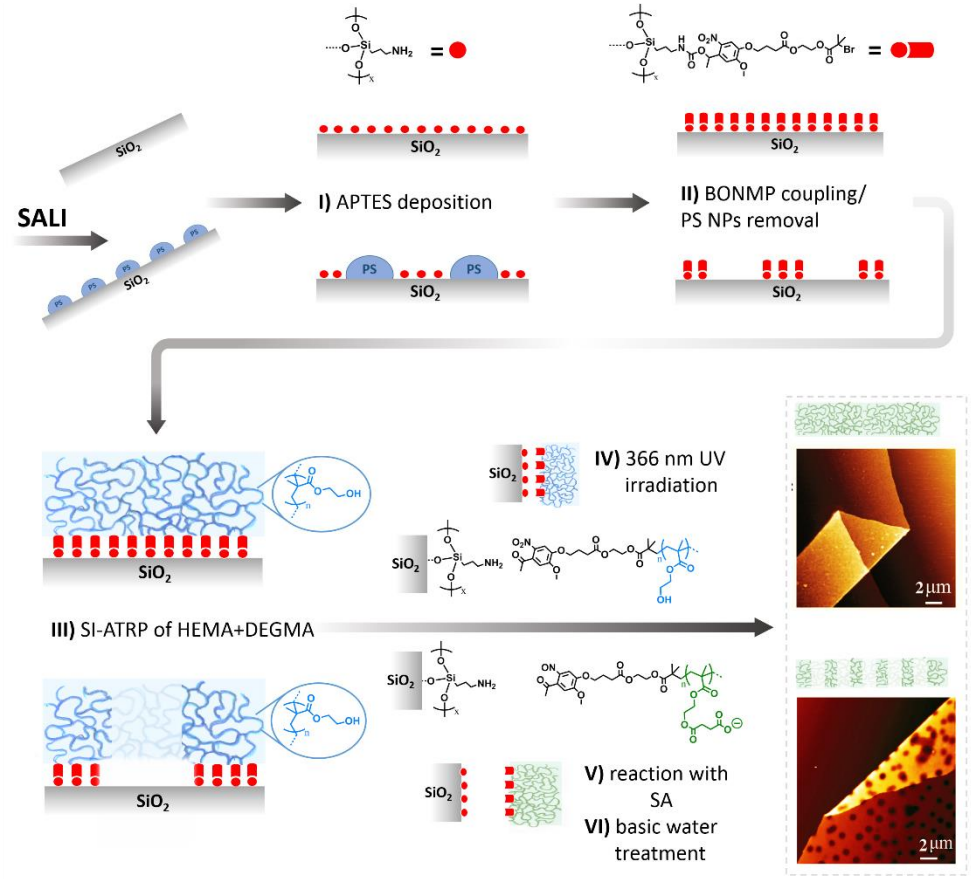

Figure 1. Synthesis of freestanding PHEMA-based hydrogel films by SI-ATRP and subsequent detachment from the initiating substrate. The formation of the photo-cleavable initiator layer on silicon oxide surfaces is performed by deposition of (3-aminopropyl)triethoxysilane (APTES) monolayer (I) and coupling of the photo-cleavable BONMB SI-ATRP initiator (II). Subsequent SI-ATRP of HEMA in the presence of 5% of DEGMA (III) produces hydrogel-brush films. 366 nm UV irradiation is applied to break the photo-cleavable anchors (IV). The modification of the PHEMA hydrogel-brush film with succinic anhydride introduces ionizable carboxylic acid function within the hydrogel films (V). Basic water treatment (pH≈10.0) allows the final lift-off of freestanding hydrogel-brush films in ultra-pure water due to osmotic pressure (VI). The fabrication of nanoporous, freestanding hydrogel-brush films is also highlighted and was carried out following similar experimental procedures. The only exception compared to the synthesis of uniform films is the nanopatterning of the initiator functions using PS NPs surface assemblies produced by SALI as masks.

Uniform, PHEMA-based, hydrogel-brush films were synthesized from BONMB-functionalized silicon substrates. In a typical procedure, SI-ATRP of HEMA in the presence of 5% of DEGMA, was performed using H_2O:MeOH 1:5 (v:v) as a polymerization medium. Following 40 hours of reaction at room temperature, a uniform PHEMA hydrogel-brush film with an average thickness of 70 ± 1 nm was obtained (PHEMA-5). The successful grafting of PHEMA was confirmed by MTR-IR spectroscopy. As depicted in Fig. 3c, the MTR profiles showed the characteristic absorption peak centered at 1741 cm^{-1}, corresponding to the ester bond of the PHEMA backbones.

In order to enable film detachment from the silicon substrate, PHEMA hydrogel-brushes were sequentially irradiated by 366 nm UV, to initiate the photo-cleavage of BONMB functions, and treated by succinic anhydride, to introduce ionizable carboxylic acid functions along the polymer backbones (Fig. 1). Immersion of the acid-modified PHEMA hydrogel films in a basic water environment provided the necessary electrostatic/osmotic force to drive the lift-off of the films as freestanding layers. In the case of PHEMA-5 (which was named PHEMA-5-SA, after the reaction with succinic anhydride), the formation of bulkier succinate groups following reaction with succinic anhydride was evidenced by an increase of dry film thickness of 35%, reaching a total thickness of 95 ± 1 nm. Consistent with these observations, the MTR-IR spectrum of PHEMA-5-SA showed a marked increase in the intensity of C=O stretching band at 174 cm^{-1} (Fig. 3d), which was related to the newly formed succinate ester groups.

Immersion of PHEMA-5-SA in aqueous solutions at pH values above the pKa of the polymer (which is around 8.0)[18] caused deprotonation of the succinic acid moieties along the brush backbones. Under these conditions, electrostatic repulsion between neighboring chains triggers expansion and profuse swelling of the films. Thus, the densely grafted chains constituting PHEMA-5-SA films are subjected to additional osmotic pressure owing both to a high counter-ion

concentration and electrostatic repulsion between the brush chains.[22] The mechanical tension generated within the brush when immersed in this environment, following UV-initiated cleavage of the initiator-derived anchors, induced the effective lift-off of the intact films (Fig. 4).

It is also noteworthy that solely treating the system with basic water (pH≈10), followed by immersion in ultra-pure water, did not lead to film detachment (as shown in Fig. 4a, where an optical micrograph of a substrate-bound film after basic water treatment is reported). Hence, the electrostatic and osmotic effects alone were not sufficient to break the covalent bonds between PHEMA-5-SA and the underlying silicon oxide surface, in the absence of a prior photolytic cleavage (Fig. 4 and Supporting Information for details).

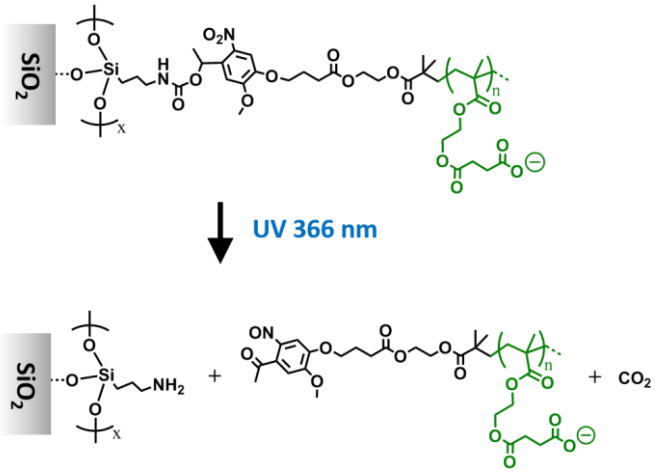

Figure 2. The photo-cleavage reaction of BONMB initiator.

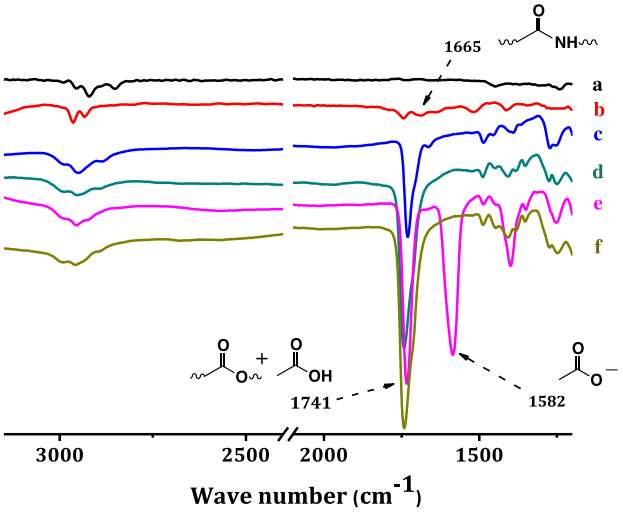

Figure 3. MTR-IR Spectra of APTES-modified silicon substrates (a); BONMB-functionalized silicon surfaces (b); PHEMA-5 (c);PHEMA-5-SA (d); PHEMA-5-SA after incubation in K2CO3 aqueous solution (pH≈10) (e); PHEMA-5-SA after incubation in HCl aqueous solution (pH≈2) (f).

Following detachment from the silicon oxide surfaces, freestanding PHEMA-5-SA hydrogel-brushes were suspended in ultra-pure water and subsequently re-deposited on freshly cleaned silicon oxide substrates (Fig. S2†). These films were characterized by tapping-mode AFM, in order to investigate

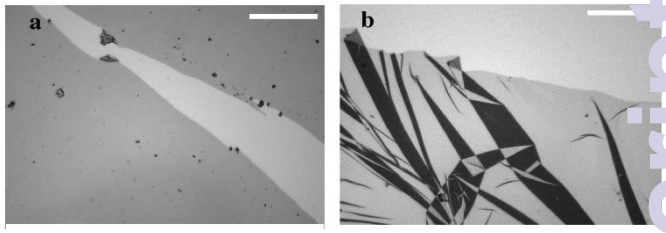

Figure 4. Optical micrographs depicting PHEMA-5-SA hydrogel-brush films with an average dry thickness of 90 nm grafted from silicon oxide substrates and exposed to only basic water treatment (a) and to 16 hours of UV irradiation followed by immersion in basic solution (pH ≈10) and final rinsing with ultra-pure water (b). In (a) the polymer films are still bound to the underlying substrate; the presence of the brush-hydrogel was highlighted by mechanically scratching the surface with plastic tweezers, thus exposing the underlying silicon oxide substrate. In (b) freestanding membranes are shown. The scale bars correspond to 50 µm.

their surface morphology and determine their average thickness (Fig. S3†). Film thickness was measured as the step height between the deposited freestanding films and the underlying substrate. As reported in Fig. S3†, an average 2.5-3-fold thickness reduction was observed for all the samples following detachment. This was presumably due to hydrogel lateral expansion and mechanical relaxation after detachment from the substrate. The observed marked increment in film area was consistent with this hypothesis.

In order to investigate the mechanical properties of PHEMA-5-SA hydrogel membranes, 70-nm-thick freestanding films were re-deposited on flat titania substrates incorporating circular pores with an average diameter of 300 nm (see Experimental Section and Supporting Information for details regarding the fabrication of these supports). AFM indentation[29,30] was performed on the areas of the PHEMA-5-SA that spanned the pores (Fig. 5). The subsequently obtained force-vs-indentation (f-i) profiles allowed the 2D modulus to be estimated, along with the pre-tension and breaking strength of the layers (a representative f-i profile is reported in Fig. 5c). As shown in Figure 3, membrane breaking was observed at between 160 and 190 nm of indentation depth, corresponding to 1.8-2.1 µN of applied force. From these values, the 2D elastic modulus could be estimated using the method described by Ruiz-Vargas et al.,[30] employing the following equation:

$$F = 2\pi\sigma d[\ln(a\, r^{-1})]^{-1} + E(q\, d^{3})a^{-2} \qquad \text{(Eq. 1)}$$

where, σ and E are the 2D membrane pre-tension and 2D effective Young's modulus, respectively. The parameters, d, a and r, are the vertical deflection, membrane radius (which corresponded to the radius of the underlying pore), and the AFM tip radius, respectively. q is a parameter that depends on the Poisson's ratio. By fitting the initial 50% of the f-i curves to the above equation (as exemplified in Fig. 5c), the pretension and the 2D modulus of PHEMA-5-SA were calculated to be 0.6 ± 0.2 and 6.5 ± 3.8 N m^{-1}, respectively. Taking film thickness into account, a Young's modulus (E^{Young}) of 101 ± 25 MPa was obtained. This value is an order of magnitude lower than the bulk modulus of PHEMA in a dry state (~ 1 GPa).[31] This confi

the previously reported observation that the mechanical behaviour of ultrathin, freestanding films is different from that of the corresponding bulk materials.[32]

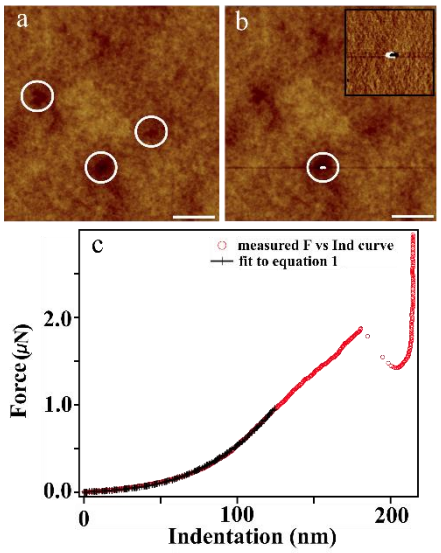

Figure 5. AFM tapping-mode micrographs depicting a PHEMA-5-SA freestanding film deposited on a porous substrate that incorporates 300 nm diameter pores. The surface of the freestanding hydrogel is shown before (a) and after (b) AFM indentation. The white circles in (a) indicate the positions where the freestanding hydrogel covers the pores before indentation. In (b), the white circle and the zoomed-in micrograph in the inset highlight the hydrogel surface covering an underlying pore after AFM indentation. In (c) a representative f-i curve obtained for PHEMA-5-SA is reported (normal spring constant of the cantilever used as indenter 25.0 N m^{-1}). The breaking of the membrane was recorded at applied forces of around 1.8 μN. The membrane pre-tension and 2D modulus obtained in this experiment were 0.4 and 9.1 N m^{-1}, respectively. The solid black line indicates the fit to Equation 1. The fitting interval taken into consideration was included between 0 and 150 nm.

Fabrication of Freestanding Nanoporous Membranes

In order to fabricate freestanding, PHEMA-SA hydrogel-brush films that incorporate controlled porosities, we performed SI-ATRP from BONMB-patterned samples. Nanopatterned initiator layers were obtained by first depositing PS NP assemblies by SALI on silicon oxide surfaces (Fig. 6a and S4†). The method exploits the trapping of charged hydrophobic nanoparticles at a water/oil interface to obtain non-close-packed nanoparticle monolayer arrays with tunable inter-particle distance. In the specific case of our experiments, different amounts of 100, 200 and 500nm amidine-terminated polystyrene latex particles were spread at a water/hexane interface of fixed area. Electrostatic repulsion at the interface prevents particle aggregation and the area density at the interface sets the monolayer coverage. Transfer of the interfacial monolayers is achieved by a modified Langmuir-Schaefer deposition, where the hydrophilic, negatively charged substrate crosses the oil/water interface at a 30° angle. Electrostatic attraction and, subsequently, van der Waals attraction ensure sufficient particle adhesion for a successful transfer, preventing aggregation induced by capillary forces during substrate extraction and drying (more details on the procedure are found in the Experimental Details). Following deposition, the NP assemblies were thermally treated in order to increase and homogenize the contact area between each particle and the substrate (Fig. S4†), APTES monolayers were subsequen deposited from the vapor phase, selectively functionalizing th exposed areas of the silicon oxide surface (Fig. 1). The PS NP were then removed by sonication in toluene, followed b incubation of the patterned APTES-functionalized surface i BONMB solution. This allowed the selective coupling of photo-cleavable initiators to the areas of exposed APTES, maintainin the previously patterned areas in an unfunctionalized state. SI-ATRP of HEMA was then carried out in the presence of 5% o DEGMA, followed by derivatization with SA. This yielded PHEMA-5-SA hydrogel-brush films that incorporated nanopores with diameters and surface densities corresponding to those o the NP assembly initially used as a template for initiato patterning (Fig. 6).

Assemblies of PS NPs of diameters of 500, 200 and 100 nm, an different NP spacing, generated nanopores through PHEMA-5-SA films with comparable diameters and coverages (Fig. 6). nanopores extended through the entire hydrogel-brush film exposing the underlying silicon surface. For confirmation, th depth was measured by tapping mode AFM and compared to the average dry film thickness recorded by ellipsometry on unpatterned PHEMA-5-SA hydrogel-brush synthesized from uniformly initiator-functionalized surface (Fig. 7). In the case of nanoporous films generated by 500 nm and 200 nm PS particle (Fig. 7a and 7b), the measured depth of nanopores agreed ver well with the film thickness obtained by ellipsometry. Additionally, the flat-bottom profiles shown in the AFM cross-sections are consistent with the exposure of a uniform silicon oxide surface.

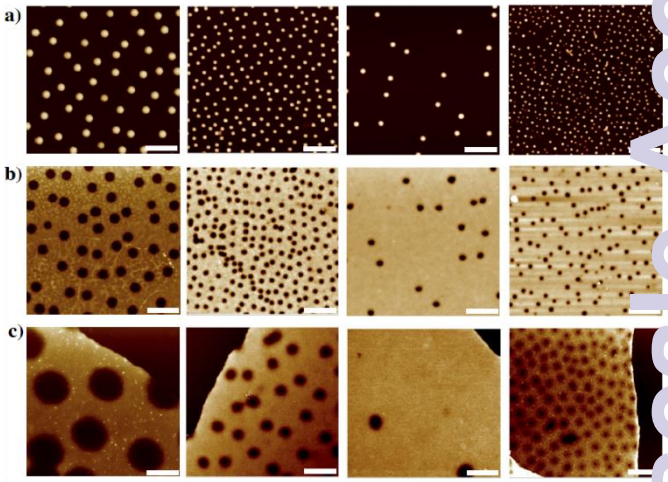

Figure 6. AFM tapping mode micrographs depicting (a) PS particles with different diameters absorbed on silicon substrates: from left to right 500 nm, 200nm with high density, 200 nm with low density and 100nm; (b) surface-grafted porous films with different pore diameters and spacings synthesized from particle-patterned substrates as in (a); free-standing nanoporous films (c) with different pore diameters and densiti generated by lift-off of surface-grafted porous films reported in (b). All scale bars correspond to 2.0 μm.

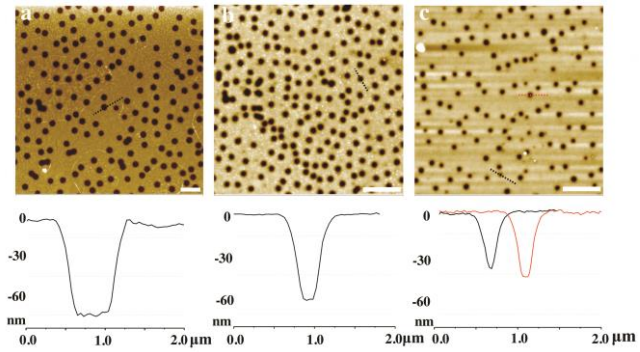

Figure 7. AFM tapping mode micrographs displaying surface-grafted PHEMA-SA hydrogel-brush films with holes generated by (a) 500 nm, (b) 200 nm and (c) 100 nm PS NPs assemblies. The representative cross-sections of the holes are indicated by coloured segments on each image. The scale bar in the graphs correspond to 2.0 µm.

Nanoporous PHEMA-5-SA films generated from 100 nm NP assemblies (Fig. 7c) presented holes with variable width, presumably due to particle polydispersity. In these cases, the cross-section over the smaller pores did not reveal a flat, underlying silicon oxide surface. This could be due to the high aspect ratio for these pores, which did not allow a faithful profiling by the tapping-mode AFM tip.

The detachment of nanoporous PHEMA-5-SA films was performed following the same procedures that were previously described for the unpatterned hydrogel-brush films. Also in these cases, the thickness of the freestanding membranes decreased between 2.5 to 3.0 times compared to the surface-grafted analogues before detachment. Simultaneously, the diameters of pores increased by a similar magnitude compared to the starting pores, due to lateral stretching of the films during lift-off. Following deposition of the detached membranes on different silicon oxide substrates, folded areas of films could be observed, as reported in Fig. S5†. Direct observation of the nanopore profiles from both sides of the freestanding films confirmed the presence of open holes throughout the membrane structure.

The pH-responsive character of nanoporous PHEMA-5-SA membranes allowed the variation of nanopore size in response to changes in the pH in aqueous medium. In order to confirm this, we incubated PHEMA-5-SA membranes in aqueous solutions with different pH values, alternatively below (pH≈2) and above (pH≈10)—the pKa of the polyacid backbones. Representative tapping-mode AFM micrographs of the films following different pH treatments are provided in Fig. 8. Incubation in basic water (pH≈10) caused opening of the nanopores due to electrostatic repulsion between the charged carboxylate anions. In this state, the PHEMA-5-SA membrane showed an average thickness of 40 ± 1 nm and nanopores with typical diameters ranging from 100 to 150 nm (Fig. 8a and 8c). Subsequent immersion of this film into acidic water (pH≈2) induced a general shrinking of the membrane, which reached an average thickness of 20 ± 1 nm, while the diameter of the nanopores decreased to few tens of nanometers (visible in the detail of Fig. 8b). It is noteworthy that the transition was always reversible and both film thickness and nanopore diameter could be restored following incubation in basic water.

Thus, the swelling characteristics of freestanding hydrogel-brush membranes responded to the pH of the medium and induced a variation of film morphology that could be exploited to tune membrane nanoporosity.

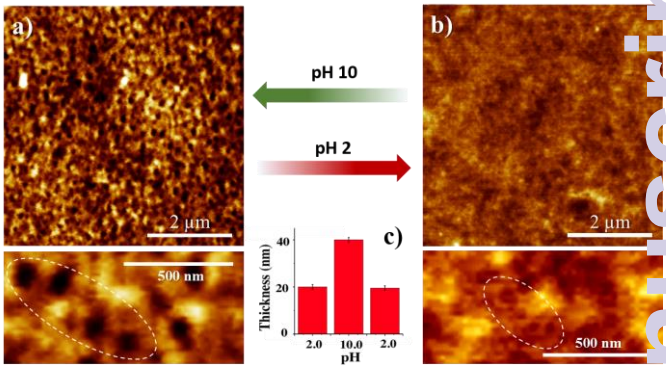

Figure 8. AFM micrographs displaying freestanding nanoporous dry films after: (a) basic (pH≈10.0) and (b) acid (pH≈2.0) treatments. In the zoomed-in micrographs below (a) and (b) the morphology changes of a series of nanopores following treatment with water at different pH values are highlighted. The white circles indicate 4 nanopores following basic (a) and acid (b) water treatments. The inserted pillar graph in (c) indicates the change of film thicknesses following the different pH treatments.

Conclusions

Freestanding, ultrathin membranes based on hydrogel-brush templates were synthesized by a combination of SI-ATRP, photo-cleavage of surface-attached initiators and pH-induced swelling. Controlled nanoporosities were introduced by performing polymerization on initiator layers that had been previously nanopatterned by means of NP assemblies. Controlled variation of nanopore size and density in the freestanding membranes was thus enabled by adjustment of the initial assembly characteristics. The mechanical and morphological properties of the generated films were comprehensively studied by AFM techniques. Due to the presence of weak polyacid functions throughout the film architecture, freestanding membranes showed pH-responsive properties that allowed the control of film thickness and pore size in response to a variation of the pH in the medium.

The results reported in this work demonstrate how SI-ATRP performed from nanostructured materials allows the fabrication of chemically robust, thin polymer films with finely controlled morphologies and functional character. The compatibility of these methods with a large variety of chemistries could stimulate further applications in the development of scaffolds for tissue engineering, or alternatively, the designing of ultrathin components for membrane technology.

Experimental Details

Synthesis of the photo-cleavable SI-ATRP initiator.

A detailed description of the synthesis and characterization of the BONMB photo-cleavable initiator is the object of a dedicated publication.[33] We report here in brief the main synthetic steps, which are summarized in Fig. S7†.

2-((2-bromo-2-methylpropanoyl)oxy)ethyl 4-(4-acetyl-2-methoxy-5-nitrophenoxy)butanoate (compound 5, Scheme S1). Compound 1 was commercially available, while compounds 2 to 4 were synthesized according to a previously described method.[34] The typical procedure for the synthesis of 5 is as follows: 4 (0.8 g, 2.7 mmol), N,N-dicyclohexylcarbodiimide (DCC) (0.8 g, 3.9 mmol), and 4-dimethylaminopyridine (DMAP) (39.0mg, 0.32mmol) were dissolved in 20 ml of THF anhydrous, and then 2-hydroxyethyl 2-bromo-2-methylpropanoate[35] (0.58g, 2.7mmol) in 0.5 ml of THF anhydrous were added. After stirring for 24h, the precipitate was filtered and the solvent removed under vacuum. The obtained crude product was dissolved in ethyl acetate (EtOAc), then washed with HCl-acidified brine solution (pH≈2.0), dried by anhydrous $MgSO_4$, and finally evaporated to yield a brown viscous oil. Chromatography on silica gel (ethyl acetate: hexane= 1: 1) afforded compound 5 (1.2 g, 90% yield) as a light brown viscous oil. 1H NMR (300MHz, d-$CDCl_3$(δ 7.20)): δ (ppm) 7.54 (s, 1H), 6.68 (s, 1H), 4.31 (m. 4H), 4.09 (t, 2H), 3.89 (s, 3H), 2.52 (t, 2H), 2.43 (s, 3H), 2.14 (quint, 2H), 1.86 (s, 6H). 13C NMR (300MHz, d-$CDCl_3$(δ 77.05)): δ (ppm) 200.02, 172.49, 171.47, 154.31, 148.45, 138.40, 132.91, 108.81, 108.07, 68.38, 63.49, 61.88, 56.61, 55.41, 30.67, 30.39, 24.12, 24.03. IR (cm^{-1}): 2951.6, 1738.3, 1712.9, 1515.3, 1220.6, 1153.6.

Synthesis of 2-((2-bromo-2-methylpropanoyl)oxy)ethyl 4-(4-(1-hydroxyethyl)-2-methoxy-5-nitrophenoxy)butanoate (6). To a solution of 5 (2.80 g, 5.7 mmol) in 140 ml MeOH at 0 °C was added $NaBH_4$ (0.12 g, 3.1 mmol) under gentle stirring. A small amount of gas was generated and the mixture was allowed to react for 20 min. Reduction of the ester bond by $NaBH_4$ is observed if the reaction is carried out at room temperature. The reaction was terminated by addition of 100 ml of NH_4Cl (aq. sat.) and the mixture was extracted with EtOAc. The organic phase was finally dried with $MgSO_4$ anhydrous and evaporated. The crude product was further purified by passing it through a silica gel column with hexane and EtOAc (v/v= 1:1) as eluent, to yield a light brown viscous oil (1.4g, 56% yield). 1H NMR (300MHz, d-$CDCl_3$(δ 7.20)): δ (ppm) 7.50 (s, 1H), 7.23 (s, 1H), 5.49 (quint. 1H), 4.31 (m, 4H), 4.05 (t, 2H), 3.91 (s, 3H), 2.52 (t, 2H), 2.18 (d, 1H), 2.13 (quint, 2H), 1.85 (s, 6H). 1.48 (d, 3H). 13C NMR (300MHz, d-$CDCl_3$(δ 77.04)): δ (ppm) 172.62, 171.49, 154.14, 146.92, 139.58, 136.98, 109.15, 108.76, 68.20, 65.79, 63.52, 61.82, 56.36, 55.39, 30.67, 30.46, 24.30, 24.23. IR wavenumber (cm^{-1}): 2973.6 1744.1, 1525.6, 1263.8,1159.4.

Synthesis of 2-((2-bromo-2-methylpropanoyl)oxy)ethyl 4-(4-(1-((((2,5-dioxopyrrolidin-1-yl)oxy)carbonyl)oxy)ethyl)-2-methoxy-5-nitrophenoxy)butanoate (BONMB-succinimidyl ester). 0.51 g (2.0mmol) N,N'-disuccinimidyl carbonate was added to a mixture of 6 (0.25 g, 0.5 mmol) and DMAP (33 mg, 0.27 mmol) in 10 ml anhydrous CH_3CN, the mixture was stirred for 24h in darkness at 40°C. The completion of the reaction was determined by thin-layer chromatography (TLC), with hexane/ EtOAc (50/50%) as mobile phase. The solvent was finally evaporated and the obtained viscous solid was purified by chromatography on silica gel (ethyl acetate: hexane= 1: 1). BONMP-succinimidyl ester (0.50 g, 76% yield) was obtained as a light brown viscous oil. 1H NMR (300MHz, d-$CDCl_3$(δ 7.19)): δ (ppm) 7.57 (s, 1H), 6.99 (s, 1H), 6.42 (q. 1H), 4.31 (m, 4H), 4.06 (t, 2H), 3.97 (s, 3H), 2.73 (s, 4H), 2.52 (t, 2H), 2.13 (quint, 2H), 1.85 (s, 6H). 1.68 (d, 3H), 1H NMR (300MHz, d-CDCl3(δ 77.04)) δ (ppm) 172.59, 171.49, 168.45, 154.63, 150.59, 147.67, 139.20, 131.26, 109.17, 107.36, 68.18, 63.53, 61.84, 56.52, 55.42, 30.66, 30.43, 25.44, 24.18, 21.96. IR (cm^{-1}): 2962.0, 1819.2, 1789.2, 1738.3, 1519.9, 1216.0, 1080.8.

Deposition of photo-cleavable BONMB SI-ATRP initiator on silicon substrates.

Silicon (100) wafers (Si-Mat Silicon wafers, Germany) were cut into 2.5× 4.0 cm2 pieces, which were cleaned by sonication in 2-propanol (3 × 10 min), and finally incubated in a UV/ozone chamber for 30 min (UV/Ozone ProCleaner TM and ProCleanerTM Plus, BioForce, IA, USA). In order to immobilize BONMB initiator on silicon substrates, these were first functionalized with amino groups by functionalization with (3-aminopropyl) triethoxysilane (APTES) via vapor-phase deposition.25 Coupling of BONMB functions was performed by reacting BONMP-succinimidyl ester on an APTES-modified silicon oxide substrates in dry THF (10 mg/ml). The amount of initiator immobilized on the substrates could be adjusted by controlling the reaction time. Following the reaction, the samples were briefly sonicated in THF and finally dried dried under a stream of N_2.

SI-ATRP of HEMA. BONMB-modified substrates were subsequently used for SI-ATRP of HEMA. All polymerization reactions were carried out in a Schlenk line under nitrogen atmosphere. In a typical procedure, 2,2'-bipyridine (0.88 mmol, 0.14 g, Acros, Germany) was dissolved in HEMA (2ml, 0.017mol, Sigma-Aldrich, Germany), 1.9 ml methanol and 0.4 ml water, with 0.1 ml di(ethylene glycol) dimethacrylate (99.9%, Sigma-Aldrich, Germany) as crosslinker. The solution was subjected to three freeze-pump-thaw circles (15 min each), to remove the dissolved oxygen, and was then transferred to another flask containing CuCl (0.39 mmol, 38.8 mg, Sigma-Aldrich, Germany, 99.9%) and CuCl2 (0.044 mmol, 5.9 mg, Sigma-Aldrich, Germany, 99.9%). After stirring the mixture for 15 min at room temperature, the dark brown mixture was transferred to flasks containing freshly prepared, initiator-modified silicon substrates. The polymerization was carried out at room temperature for the desired time. After these steps the wafers were taken out from the polymerization solution, extensively washed in DMF and dried in a stream of nitrogen gas.

Lift-off of PHEMA hydrogel-brush films from silicon substrates. PHEMA-based hydrogel-brush films were first exposed to 366 nm UV light with an intensity of 2.8 mW/cm2 for the necessary time. The substrates were then immersed into a pyridine solution of succinic anhydride overnight (0.1 g ml^{-1}, Sigma-Aldrich, Germany, 99.9%). The resulting PHEMA-SA films were dipped into a K_2CO_3 aqueous solution (pH≈10) followed by incubation in ultra-pure water to assure the lift-off from the silicon surface of the hydrogel-brushes as freestanding films.

Measurement of mechanical properties of detached hydrogel-brush membranes.

The mechanical properties of freestanding hydrogel-brush membranes were measured by AFM indentation. Briefly, the freestanding films were initially dispersed in ultra-pure water and subsequently transferred onto porous titania (see Supporting Information for their preparation). Indentation experiments were performed using MFP3D (Asylum Research, Santa Barbara) AFM. The spring constant of the cantilevers (OMCL-AC160TS, Olympus, Japan) were measured using Get Real calibration option in the AR software which combines both thermal noise method and Sader's method[36,37] (By using this method, pressing against a hard surface to obtain the sensitivity can be avoided, with the result that the tip remains very sharp prior to the first indentation).

Assembly of PS particles on silicon substrates and fabrication of freestanding nanoporous membranes.

A 10x10 mm2 Si wafer was lowered into a 50 ml polypropylene centrifuge tube (TPP AG, Switzerland) filled with 40 ml of ultra-pure water (R = 18.2 Ω, TAC <6ppb) on a holder at an angle of 30° relative to the water interface. 7 ml of hexane (≥ 95%, Sigma-Aldrich) were added carefully to form a water-oil interface. Nanoparticle suspensions were prepared as 0.08% w/v suspensions of amidine polystyrene latex particles of 0.1 and 0.2 µm diameter (diluted from 4% w/v stock solutions (Life Technologies)) and as 0.16% w/v suspensions of 0.5 µm diameter amidine polystyrene latex particles (diluted from 4% w/v stock solutions (Life Technologies)).[23] The dilutions were carried out in a 60:40 mixture of ultra-pure water:2-propanol (≥ 99.8%, Sigma-Aldrich) to aid particle spreading upon deposition at the interface. 3.5 µl, 7 µl or 14 µl of suspension were injected using a syringe pump at a speed of 0.5 µl s^{-1} to the specified volume via a needle inserted through the wall of the centrifuge tube with the tip carefully positioned at the hexane-water interface. Long-range dipolar electrostatic repulsion between the charged particles drives the formation of non-close-packed particle arrays,[38] with the particle separation determined by the number of particles injected per unit area,[21] i.e. controlled by the injection volumes relative to the fixed area of the centrifuge tubes.

Following a waiting period of 5 minutes, the wafers were extracted through the hexane-water interface, and subsequently the hexane-air interface, at a speed of 25 µm s^{-1}, to deposit the particle patterns. The speed was chosen to be equal to (or lower than) the rate of hexane evaporation on the wafer upon extraction to minimize the effect of particle rearrangement when a drying meniscus is formed.

To enhance the contact of the PS NP assemblies with the silicon substrates, PS NPs with 100 nm and 200 nm in diameter were thermally treated at 120°C for 4 hours, while 500 nm PS NPs were treated at 105 °C for 4h. The assemblies were later functionalized with BONMB initiator, following the same procedure reported in the previous section.

Acknowledgements

Funding from the ETH Research Commission is gratefully acknowledged. EMB acknowledges financial support from the Swiss National Science Foundation (SNSF "Ambizione" PZ00P2-148156). LI acknowledges financial support from the Swiss National Science Foundation grant PP00P2_144646/1.

Notes and references

1 Koenig, S. P.; Wang, L.; Pellegrino, J.; Bunch, J. S. *Nat. Nanotechnol.* 2012, **7**, 728.
2 Chai, S.-H.; Nelson, K.; Bi, Z.; Chen, J.; Mahurin, S. M.; Zhu, X.; Qiao, Z.-A.; Dai, S. *Nat. Commun.* 2014, **5**, 1.
3 Kang, T. J.; Cha, M.; Jang, E. Y.; Shin, J.; Im, H. U.; Kim, Y.; Lee, J.; Kim, Y. H. *Adv. Mater.* 2008, **20**, 3131.
4 Zeng, T.; Claus, R.; Zhang, F.; Du, W.; Cooper, K. *Smart mater. and struct.* 2001, **10**, 780.
5 Fujie, T.; Matsutani, N.; Kinoshita, M.; Okamura, Y.; Saito, A.; Takeoka, S. *Adv. Funct. Mater.* 2009, **19**, 2560.
6 Borges, J; Mano, J.F. *Chem. Rev.* 2014, **114**, 8883.
7 Tang, Z.; Wang, Y.; Podsiadlo, P.; Kotov, N.A. *Adv. Mater.* 2006, **18**, 3203.
8 Andres, C.M.; Kotov, N.A. J. Am. Chem. Soc. 2010, **132**, 14496.
9 Decher G. *Science* 1997, **277**, 1232.
10 Shin, Y. J.; Kang, S. J.; Jung, H. J.; Park, Y. J.; Bae, I.; Choi, D. H.; Park, C. *ACS Appl. Mater. Interfaces* 2011, **3**, 582.
11 Jiang, C.; Markutsya, S.; Pikus, Y.; Tsukruk, V. V. *Nat. Mater.* 2004, **3**, 721.
12 Jiang, R.; Li, B.; Fang, C.; Wang, J. *Adv. Mater.* 2014, **26**, 5274.
13 Tokarev, I.; Minko, S. Multiresponsive, *Adv. Mater.* 2009, 241.
14 12.Peinemann, K.-V.; Abetz, V.; Simon, P. F. W. Nat. Mater. 2007, **6**, 992.
15 Rao, J.; De, S.; Khan, A. *Chem. Commun.* 2012, **48**, 3427.
16 Rao, J.; Ma, H.; Baettig, J.; Woo, S.; Stuparu, M. C.; Bang, J.; Khan, A. *Soft Matter* 2014, **10**, 5755.
17 Barbey, R.; Lavanant, L.; Paripovic, D.; Schüwer, N.; Sugnaux, C.; Tugulu, S.; Klok, H.-A. *Chem. Rev.* 2009, **109**, 5437.
18 Benetti, E. M.; Sui, X.; Zapotoczny, S.; Vancso, G. J. *Adv. Funct. Mater.* 2010, **20**, 939.
19 Edmondson, S.; Huck, W. T. S. *Adv. Mater.* 2004, **16**, 1327.
20 Edmondson, S.; Frieda, K.; Comrie, J. E.; Onck, P. R.; Huck, W. T. S. *Adv. Mater.* 2006, **18**, 724.
21 Amin, I.; Steenackers, M.; Zhang, N.; Beyer, A.; Zhang, X.; Pirzer, T.; Hugel, T.; Jordan, R.; Gölzhäuser, A. *Small* 2010, **6** 1623.
22 Tokarev, I.; Minko, S. *Soft Matter* 2009, **5**, 511.
23 Isa, L.; Kumar, K.; Müller, M.; Grolig, J.; Textor, M.; Reimhult, E. *ACS Nano* 2010, **4**, 5665.
24 Kang, C.; Crockett, R. M.; Spencer, N. D. *Macromolecules* 2014, **47**, 269.
25 Liu, H.-B.; Venkataraman, N. V.; Spencer, N. D.; Textor, M.; Xiao, S.-J. *ChemPhysChem* 2008, **9**, 1979.
26 Liu, H.-B.; Venkataraman, N. V.; Bauert, T. E.; Textor, M.; Xiao, S.-J. *J. Phys. Chem. A* 2008, **112**, 12372.
27 Jönsson, U.; Olofsson, G.; Malmqvist, M.; Rönnberg, I. *Thin Solid Films* 1985, **124**, 117.
28 Papageorgiou, G.; Corrie, J. E. *Tetrahedron* 1997, **53**, 3917.
29 Lee, C.; Wei, X.; Kysar, J. W.; Hone, J. *Science* 2008, **321**, 385
30 Ruiz-Vargas, C. S.; Zhuang, H. L.; Huang, P. Y.; van der Zande, A. M.; Garg, S.; McEuen, P. L.; Muller, D. A.; Hennig, R. G.; Park, J. *Nano Lett.* 2011, **11**, 2259.
31 Di Marco, G.; Lanza, M.; Pieruccini, M. *Il Nuovo Cimento D* 1994, **16**, 843.
32 Xia, W.; Keten, S. *J. Mater. Res.* 2015, **30**, 36.
33 Kang, C.; Crockett, R. M.; Spencer, N. D. *(submitted)*

34 Holmes, C. P. *J. Org. Chem.* 1997, **62**, 2370.
35 Tao, P.; Li, Y.; Rungta, A.; Viswanath, A.; Gao, J.; Benicewicz, B. C.; Siegel, R. W.; Schadler, L. S. *J. Mater. Chem.* 2011, **21**, 18623.
36 Butt, H.-J.; Jaschke, M. *Nanotechnology* 1995, **6**, 1.
37 Green, C. P.; Lioe, H.; Cleveland, J. P.; Proksch, R.; Mulvaney, P.; Sader, J. E. *Rev. Sci. Instrum.* 2004, **75**, 1988.
38 Pieranski, P. *Phys. Rev. Lett.* 1980, **45**, 569.